Int. Conference of Plasticity, Damage & Fracture 2026
January 6, 2026, Geelong, Australia

Statistical Inference and Uncertainty Quantification for BCC Crystals[1]

Hansohl Cho*, Seunghyeon Lee

Korea Advanced Institute of Science and Technology

Thao Nguyen, Darby J. Luscher, Saryu J. Fensin, John S. Carpenter

Los Alamos National Laboratory

* hansohl@kaist.ac.kr

Body-centered-cubic (BCC) materials

- BCC refractory metals in Group 5 (e.g., Ta) and 6 (e.g., Mo)
- High melting point (Mo: 2896 K, Ta: 3290 K), high strength, and corrosion resistance
- Critical applications for mechanical, thermal, and chemical extremes

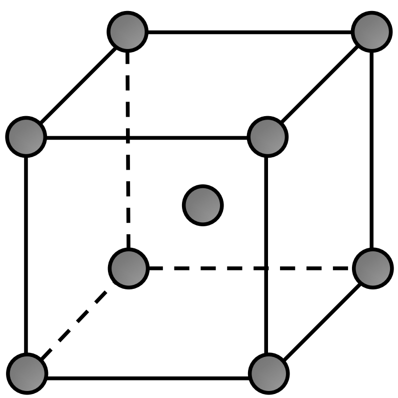

Body-centered-cubic structure

Tantalum

Molybdenum

Challenges in BCC crystal plasticity modeling

- Complex dislocation kinetics and multiple slip system families ({110}, {112}, {123})
- **Interaction between dislocations** throughout the active slip systems
- **High dimensional** parameter space
- Breakdown of the classical Schmid law

→ Challenges in unified single crystal plasticity modeling and "parameter" identification

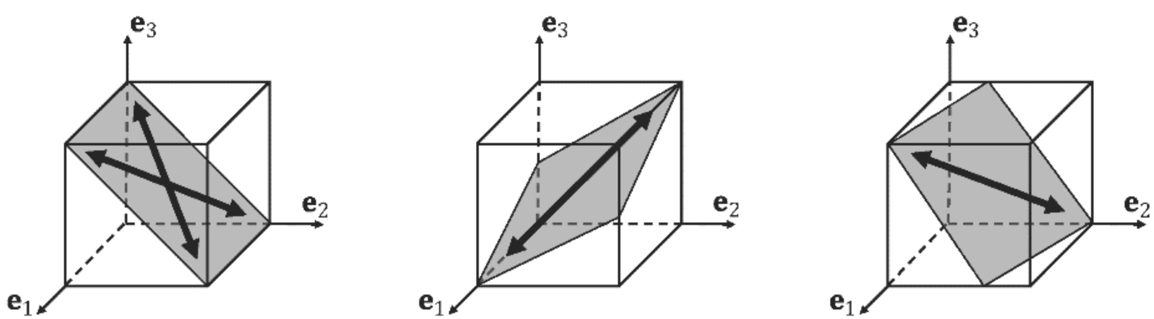

<111>{110} <111>{112} <111>{123}

< > : Slip directions
{ } : Slip planes

Slip system families for BCC single crystals

Identification of parameters in crystal plasticity models

1. Deterministic calibration:

→ Identifies a single parameter set (x^*)

→ Minimizes errors for the best fit

2. Statistical calibration (In this work):

→ Infers probability density functions of the parameters

→ Advantage: **Identifies robust parameter regions applicable to various conditions**

Bayesian calibration

- Statistical approaches have been widely used for calibrating and validating complex models
- Bayesian calibration (Kennedy and O'Hagan 2001; Higdon et al. 2008)[2,3]

: Quantifies **parameter uncertainty** consistent with **observations**

Data & prior uncertainty

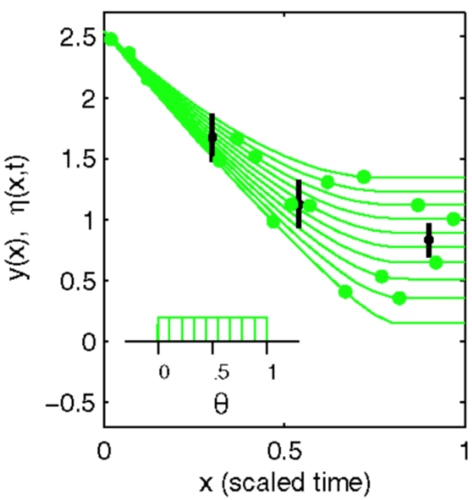

Bayes' rule:

$p(\theta \mid y) \propto$

$f(y \mid \theta)\, \pi(\theta)$

θ: **Parameter distribution**
y: Observation
η: Model prediction
f: Likelihood

Calibrated simulator prediction

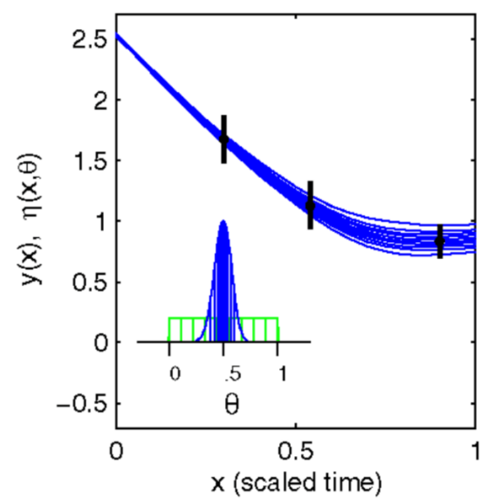

Adapted from Higdon et al.

: Observations or experimental data

: Prior responses (before calibration)

: Posterior responses (after calibration)

Bayesian calibration

- Calibration data: Uniaxial stress-strain response of single crystals (e.g., molybdenum)
- **Prior**: Uniform distributions for key parameters (to be calibrated)
- **Methodology**: Markov chain Monte Carlo (MCMC) accelerated by Gaussian-process emulator

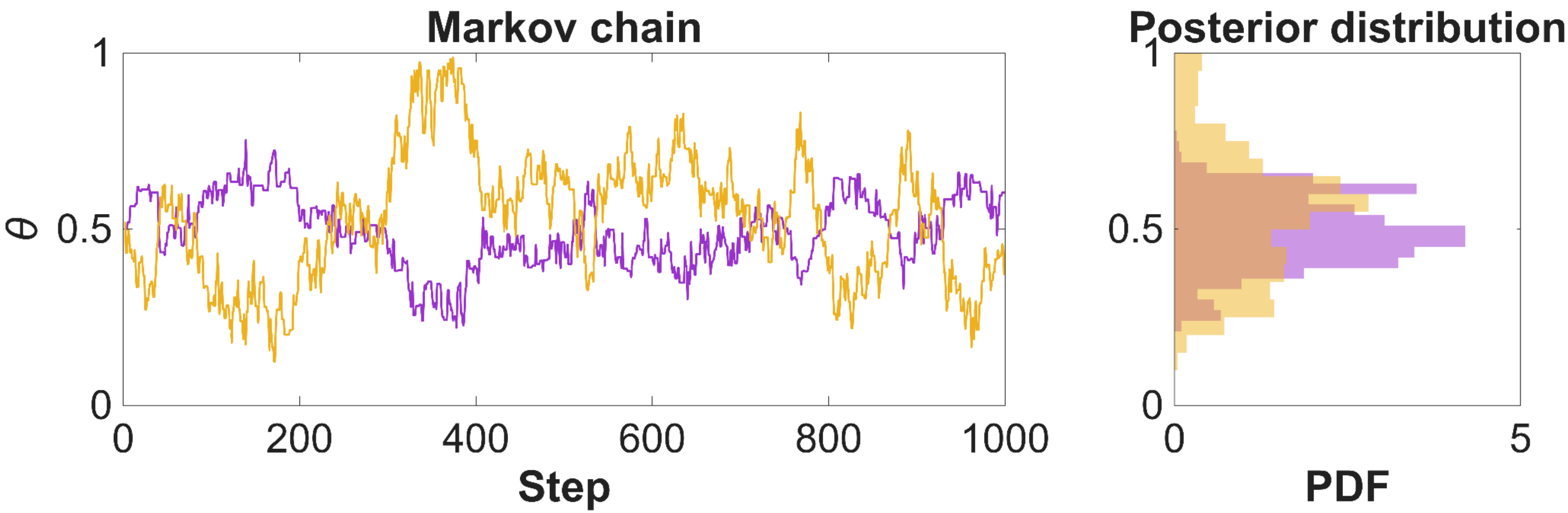

Random sampling of parameter candidate at each step

→ Accepted or rejected by the Metropolis–Hastings criterion with Bayes' rule

Our goals

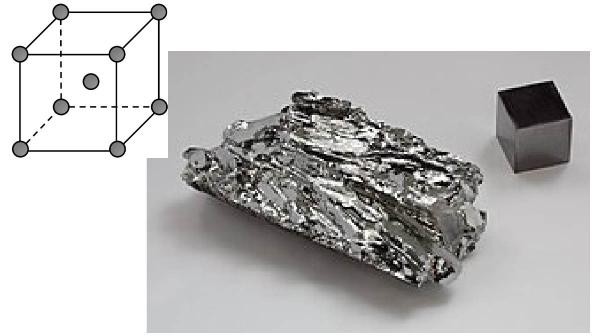

Molybdenum

- Crystal plasticity modeling of bcc molybdenum
- Statistically driven model validation and comparison
  - Model 1: Mobile dislocation kinetics-based model[4]
  - Model 2: Dislocation interaction-based model[5]

  → Identification of key model components and assumptions
- Model refinement guided by statistical inference and sensitivity information

  → What additional mechanisms are needed to account for the model discrepancy?

Two distinct single crystal plasticity models 1 and 2

- Model 1: **Nguyen, Luscher et al. 2021**[4] and earlier works
- Model 2: **Lee, Cho, Bronkhorst et al. 2023**[5] and earlier works
- Dislocation density evolution in **Model 1**

$$\rho^{\alpha} = \rho_M^{\alpha} + \rho_I^{\alpha}$$

$$\dot{\rho}_M^{\alpha} = \dot{\rho}_{\text{mult}}^{\alpha} - \dot{\rho}_{\text{ann}}^{\alpha} - \dot{\rho}_{\text{trap}}^{\alpha}$$

$$\dot{\rho}_I^{\alpha} = \dot{\rho}_{\text{trap}}^{\alpha} - \dot{\rho}_{\text{rec}}^{\alpha} \approx f_{\text{rec}}^{\alpha}\dot{\rho}_{\text{trap}}^{\alpha}$$

$$\dot{\rho}_{\text{mult}}^{\alpha} = C_M\sqrt{\rho_{\text{for}}^{\alpha}\rho_M^{\alpha}}|v^{\alpha}|$$

$$\dot{\rho}_{\text{ann}}^{\alpha} = \frac{1}{4}C_A d_A^{\alpha}(\rho_M^{\alpha})^2|v^{\alpha}|$$

$$\dot{\rho}_{\text{trap}}^{\alpha} = C_T\sqrt{\rho_{\text{for}}^{\alpha}\rho_M^{\alpha}}|v^{\alpha}|$$

- Dislocation density evolution in **Model 2**

$$\dot{\rho}^{\alpha} = \dot{\rho}_{\text{mult}}^{\alpha} - \dot{\rho}_{\text{rec}}^{\alpha} = \frac{1}{b}\left(\sqrt{\sum_{\beta} d^{\alpha\beta}\rho^{\beta}} - 2y_c^{\alpha}\rho^{\alpha}\right)|\dot{\gamma}^{\alpha}|$$

Single crystal plasticity models 1 and 2

- Flow in **Model 1**: Coupled phonon drag and thermally-activated glide

$\dot{\gamma}_{\mathrm{p}}{}^{\alpha} = b\rho_M^{\alpha} v^{\alpha}$ Orowan's relation

$v^{\alpha} = \frac{\bar{L}^{\alpha}}{t_w^{\alpha}+t_r^{\alpha}}\,\mathrm{sign}(\tau^{\alpha})$ Mean dislocation velocity

$t_w^{\alpha} = \frac{1}{f_D}\left(\exp\left[\frac{\Delta G}{k_B\theta}\left\langle 1-\left\langle\frac{|\tau^{\alpha}|-\tau_{\mathrm{a}}^{\alpha}}{\tau_{\mathrm{r}}^{\alpha}}\right\rangle^{p}\right\rangle^{q}\right]-1\right)$ Thermal activation

$v_r^{\alpha} = \frac{\bar{L}^{\alpha}}{t_r^{\alpha}} = \frac{b}{B_{\star}^{\alpha}}(|\tau^{\alpha}|-\tau_{\mathrm{a}}^{\alpha})$ with $B_{\star}^{\alpha} = \frac{B_0}{1-(v_r^{\alpha}/c_s)^2}$ Phonon drag-limited flight

- Flow in **Model 2**: Arrhenius type thermally-activated glide → Relatively simple

$\dot{\gamma}_p^{\alpha} = \dot{\gamma}_0 \exp\left(-\frac{\Delta G}{k_B\theta}\left\langle 1-\left\langle\frac{\tau_{eff}^{\alpha}}{\tau_{\mathrm{r},0}}\right\rangle^{p}\right\rangle^{q}\right)$ for $\tau_{eff}^{\alpha} > 0$, otherwise $\dot{\gamma}_p^{\alpha} = 0$;

$\tau_{eff}^{\alpha} = |\tau^{\alpha}| - \tau_{\mathrm{a}}^{\alpha}$

Single crystal plasticity models 1 and 2

- Hardening law in **Model 1**

$$\tau_{\mathrm{a}}^{\alpha} = \tau_{\mathrm{a,0}} + C_{\mathrm{for}}\, b\mu_{\star}\sqrt{\rho_{\mathrm{for}}^{\alpha}}$$ Athermal resistance due to forest hardening

$$\tau_{\mathrm{r}}^{\alpha} = \tau_{\mathrm{r,0}} + C_{\mathrm{cop}}\, b\mu_{\star}\sqrt{\rho_{\mathrm{cop}}^{\alpha}}$$ Lattice resistance due to coplanar hardening

with

$\rho_{\mathrm{for}}^{\alpha} = \sum_{\beta=1}^{n_{slip}} A_{\mathrm{for}}^{\alpha\beta}\,\rho^{\beta}$ with $\mathrm{A}_{\mathrm{for}}^{\alpha\beta} = \frac{1}{2}\left|\mathbf{n}^{\alpha}\cdot\mathbf{s}^{\beta}\right| + \frac{1}{2}\left|\mathbf{n}^{\alpha}\cdot\left(\mathbf{n}^{\beta}\times\mathbf{s}^{\beta}\right)\right|$

$\rho_{\mathrm{cop}}^{\alpha} = \sum_{\beta=1}^{n_{slip}} A_{\mathrm{cop}}^{\alpha\beta}\,\rho^{\beta}$ with $\mathrm{A}_{\mathrm{cop}}^{\alpha\beta} = \frac{1}{2}\left|\mathbf{n}^{\alpha}\times\mathbf{s}^{\beta}\right| + \frac{1}{2}\left|\mathbf{n}^{\alpha}\times\left(\mathbf{n}^{\beta}\times\mathbf{s}^{\beta}\right)\right|$

- Hardening law in **Model 2**

$$\tau_{\mathrm{a}}^{\alpha} = \tau_{\mathrm{a,0}} + \mu b\sqrt{\sum_{\beta} a^{\alpha\beta}\rho^{\beta}}$$

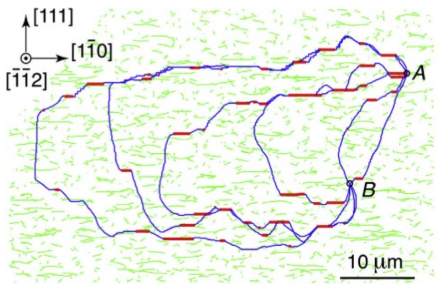

3D dislocation dynamics simulation, Madec and Kubin, 2017[6]

Parameters to be calibrated

Model 1	
p q	Shape of stress-dependent kink-pair formation energy
A	Reference thermal energy
$\dot{\gamma}_0$	Reference slip rate
C_M	Dislocation multiplication coefficient
$\rho_{0,Sat}$	Reference saturation dislocation density

- p and q govern **stress-dislocation velocity relation**
- Other four parameters govern **dislocation density evolution**

Model 2	
p q	Shape of stress-dependent kink-pair formation energy
A	Reference thermal energy
$\dot{\gamma}_0$	Reference slip rate
y_{c0}	Annihilation capture radius
k_2	Mean free path coefficient

- p, q and $\dot{\gamma}_0$ govern **stress-slip rate relation**
- $\dot{\gamma}_0, A, y_{c0}$ and k_2 govern **dislocation density evolution**

Bayesian calibration: Results

- Model 1

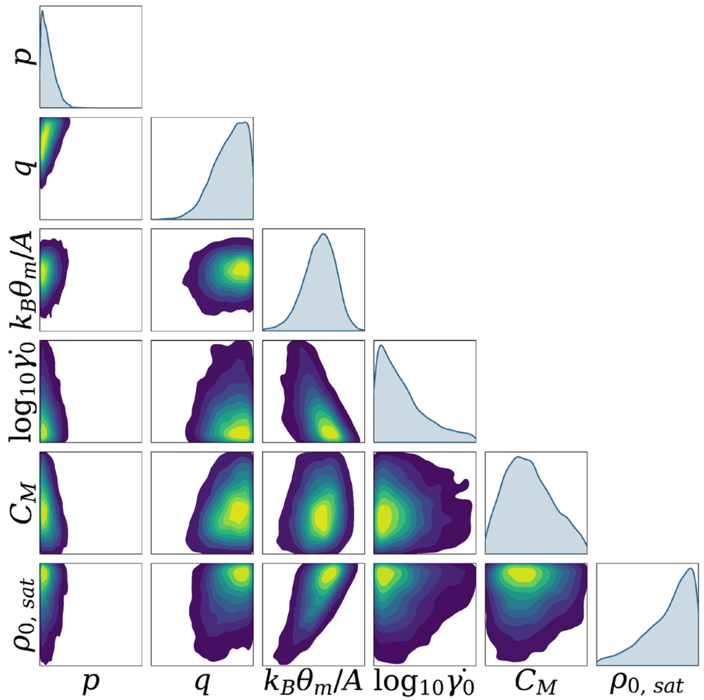

- Model 2

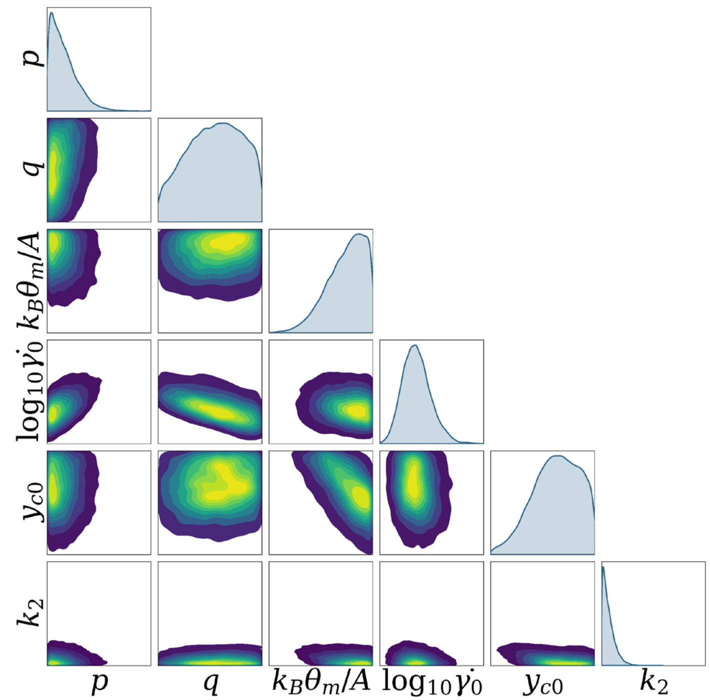

- (Diagonal) Marginal distribution: 1-D posterior probability density
- (Off-diagonal) Bivariate distribution: pairwise joint posterior probability

Bayesian calibration: Results

- Model 1 (RMSE = 54.5 MPa; CoV = 15.7%)

Strain rate: 6.5×10^{-5} to 300 s^{-1}

Temperature: 195 to 500 K

Shaded area : 90% credible interval of model prediction

Dashed line: Mean of the model response

Solid line: Experimental data

<100>

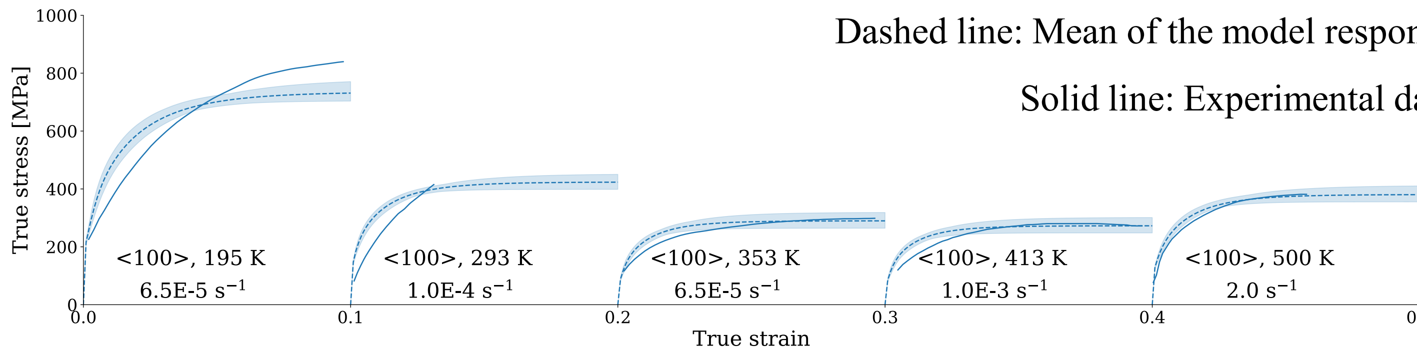

<110>

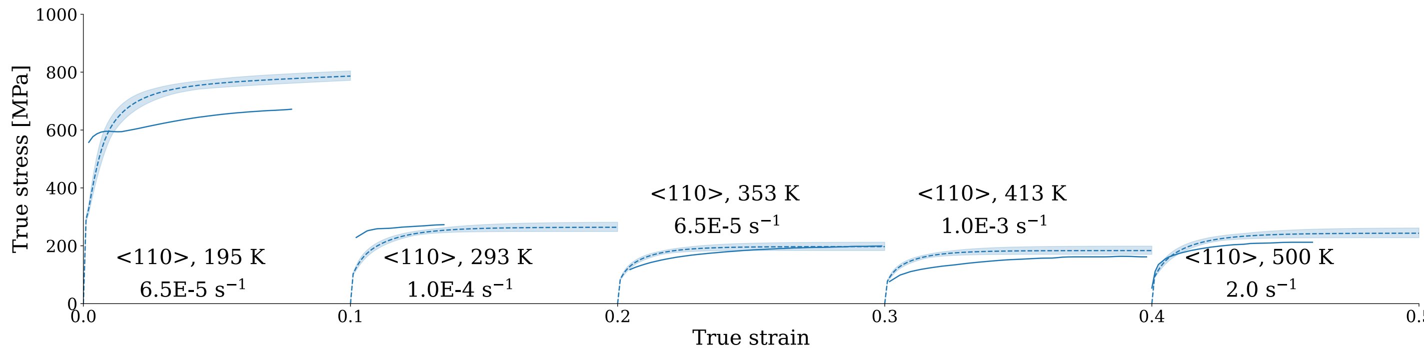

<111> &
<149>
high rates

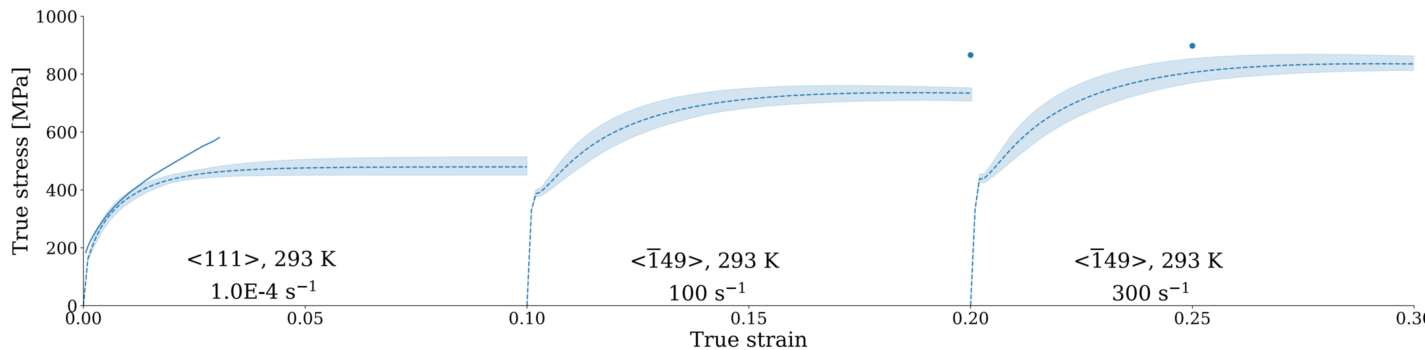

Experimental data taken from [7]-[11]

Bayesian calibration: Results

- Model 2 (RMSE = 62.3 MPa; CoV = 17.8%)

Strain rate: 6.5×10^{-5} to 300 s^{-1}

Temperature: 195 to 500 K

Shaded area : 90% credible interval of model prediction

Dashed line: Mean of the model response

Solid line: Experimental data

<100>

<110>

<111> & <149> high rates

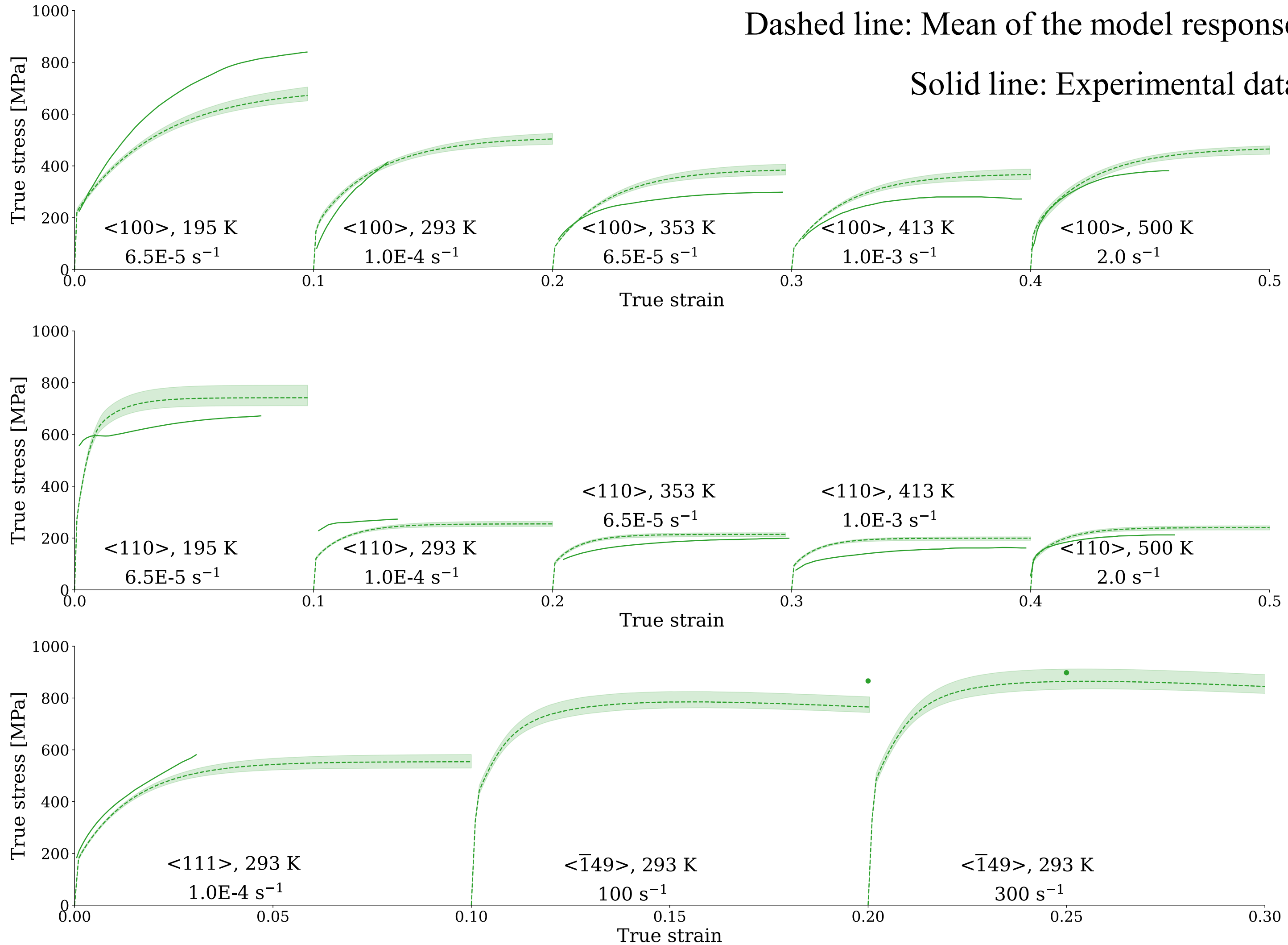

Experimental data taken from [7]-[11]

Shock responses via plate impact

- Performed probabilistic predictions of plate impact responses

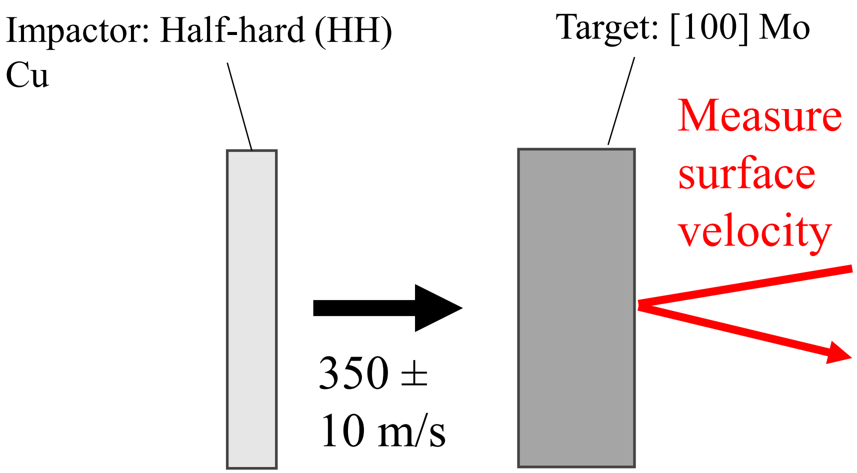

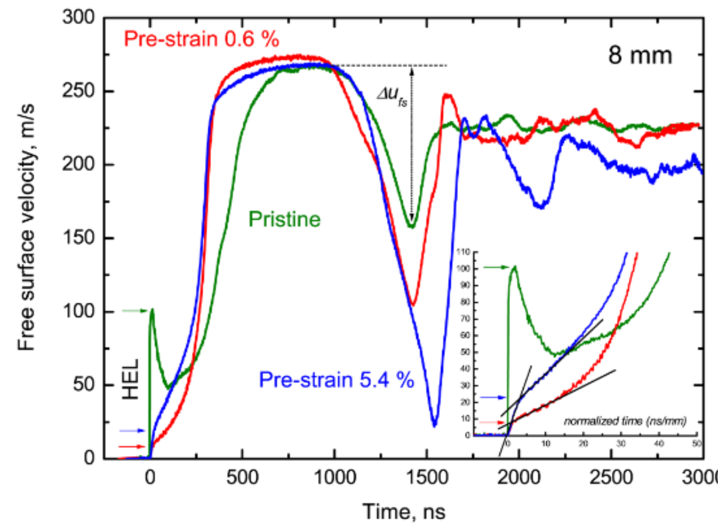

Plate impact response (free surface velocity) of **[100] Mo**[12]

- Three sources of uncertainty: **(1) impactor model, (2) target model, (3) impact velocity**

Shock responses via plate impact

Blue: 8 mm [100] Mo/ 2.5 mm Cu
Green: 4 mm [100] Mo/ 1.48 mm Cu
Orange: 2.1 mm [100] Mo/ 0.78 mm Cu

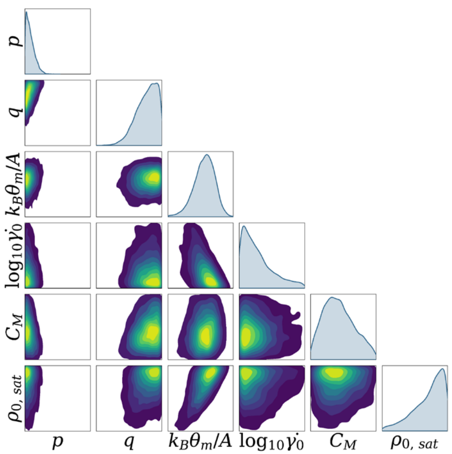

Posterior PDFs of the Mo target parameters

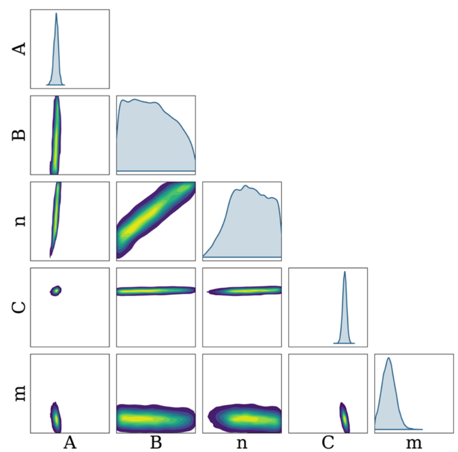

Posterior PDFs of the Cu impactor parameters

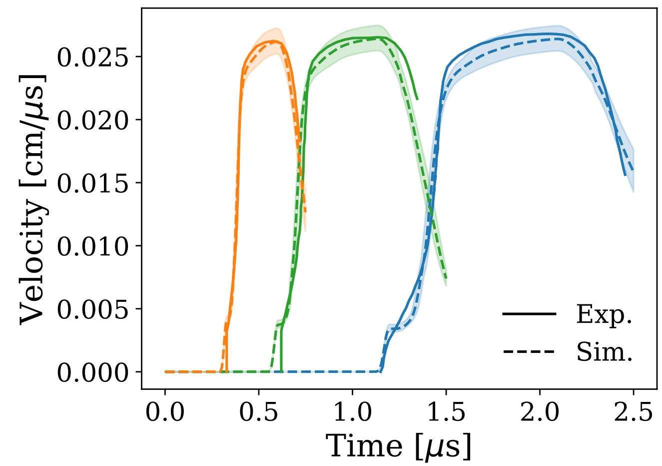

Solid line: Experimental data[12]

Shaded area: 90% credible interval of model prediction

Dashed line: Mean of the 100 responses

- **Initial dislocation density**
- **Specimen thickness** dependence

Shock responses via plate impact

B: 8 mm Mo/ 2.5 mm Cu
G: 4 mm Mo/ 1.48 mm Cu
O: 2.1 mm Mo/ 0.78 mm Cu

- **Model 1**

[100] Pristine
($\sum_\alpha \rho^\alpha = 8 \times 10^4\ \mathrm{cm}^{-2}$)

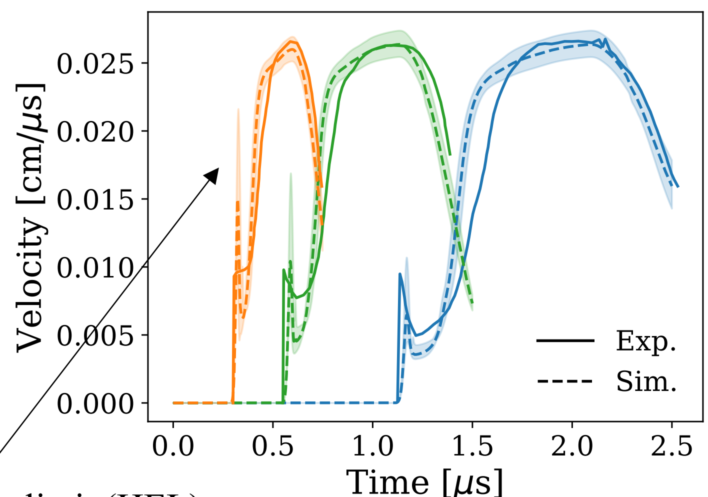

[100] Prestrain 5.4%
($\sum_\alpha \rho^\alpha = 6.5 \times 10^7\ \mathrm{cm}^{-2}$)

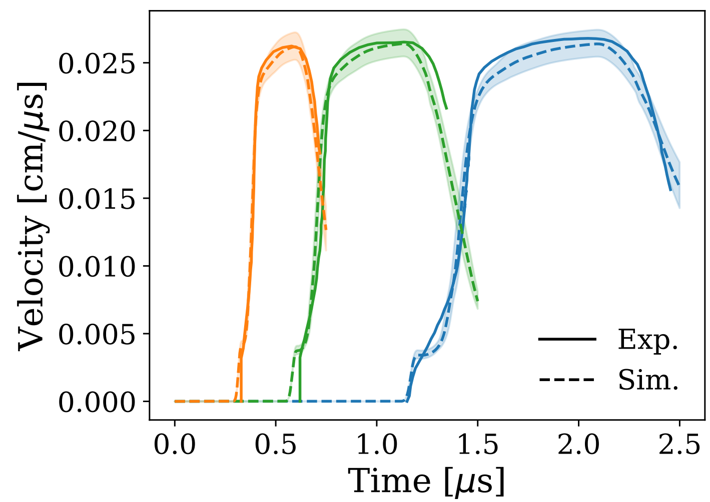

Hugoniot elastic limit (HEL)
→ Model 1 overestimates

- Goals: predicting Hugoniot elastic limit (HEL) and overall velocity rise time
- Model 1 accounts for the initial dislocation-density-dependent HEL

→ However, it overestimates the HEL for thin specimens

Shock responses via plate impact

B: 8 mm Mo/ 2.5 mm Cu
G: 4 mm Mo/ 1.48 mm Cu
O: 2.1 mm Mo/ 0.78 mm Cu

- **Model 2**

[100] Pristine
($\sum_\alpha \rho^\alpha = 8 \times 10^4$ cm^{-2})

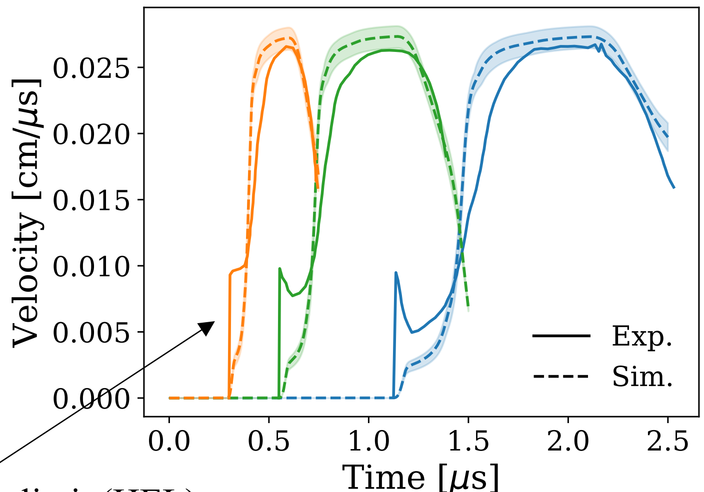

Hugoniot elastic limit (HEL)

[100] Prestrain 5.4%
($\sum_\alpha \rho^\alpha = 6.5 \times 10^7$ cm^{-2})

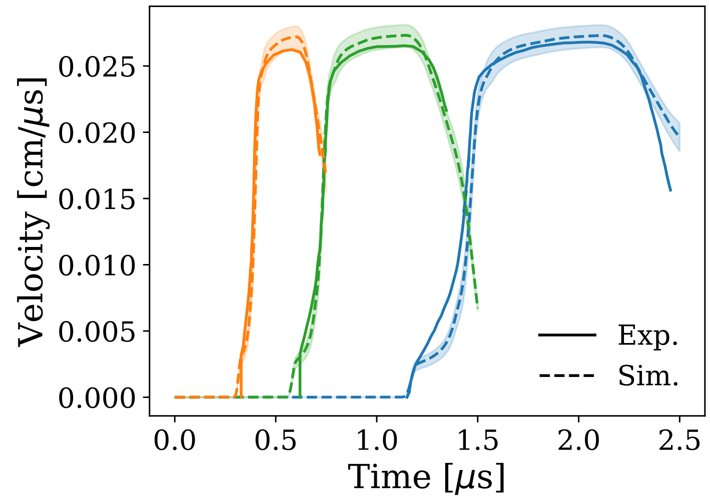

- Goals: predicting Hugoniot elastic limit (HEL) and overall velocity rise time
- Model 2 cannot account for the initial dislocation-density-dependent HEL

Global sensitivity analysis (SA)

- Variance-based global sensitivity analysis[13]

→ Which **input parameters** have the **greatest influence on the response**?

- Sensitivity (Sobol') indices

First-order: $S_i = \frac{D_i}{\mathrm{Var}[Y]}$ — D_i: Variance attributed to i-th parameter; $\mathrm{Var}[Y]$: Total variance — Influence of the i-th parameter

Second-order: $S_{ij} = \frac{D_{ij}}{\mathrm{Var}[Y]}$ — Pure interaction between i-th and j-th parameter

$$D_i = \mathrm{Var}_{X_i}\left(E_{\boldsymbol{X}_{\sim i}}[Y \mid X_i]\right)$$
$$D_{ij} = \mathrm{Var}_{X_{ij}}\left(E_{\boldsymbol{X}_{\sim ij}}[Y \mid X_{ij}]\right) - D_i - D_j$$

$$\sum_{i=1}^{d} S_i + \sum_{i<j}^{d} S_{ij} + \cdots + S_{12\cdots d} = 1$$

Global sensitivity analysis (SA)

- Global sensitivity analysis → **identify dominant mechanisms**

Compute plate impact responses from uniform parameter distributions

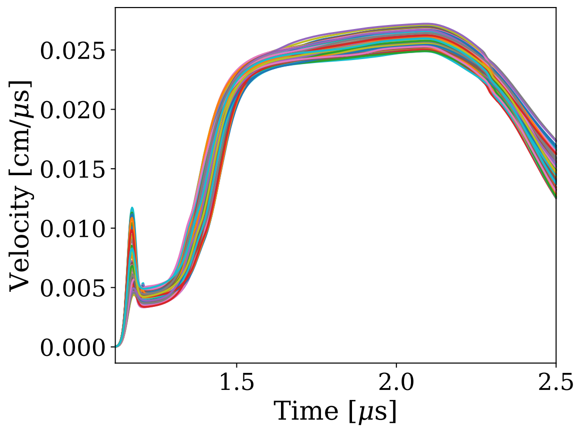

Compute sensitivity indices (S_i, S_{ij},…) at each time[14]

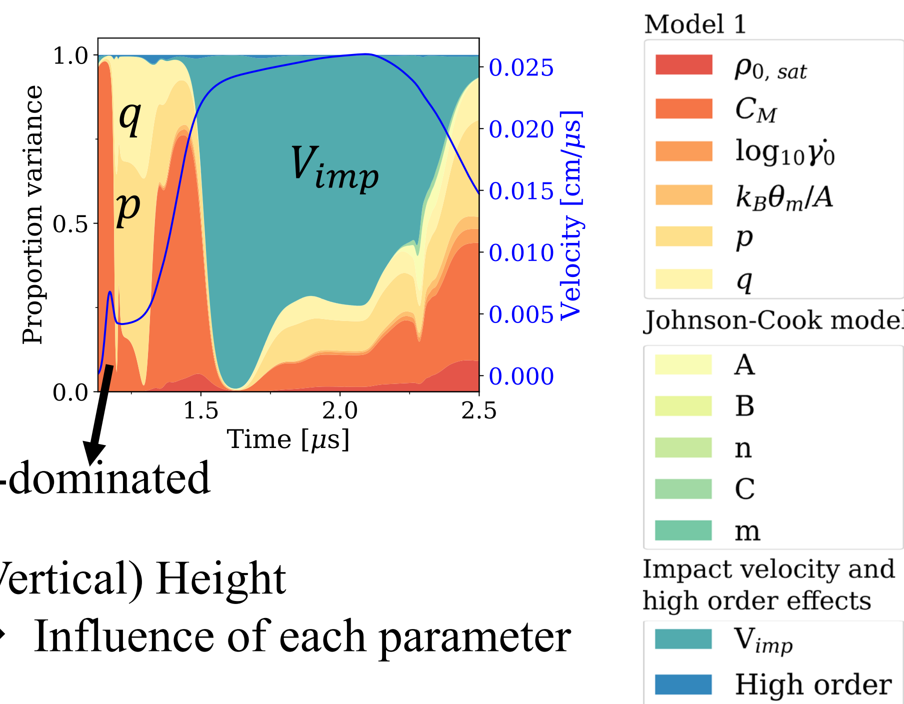

C_M-dominated

Train **spline-based surrogates** (Francom and Sansó 2020) and perform **analytical integration**

(Vertical) Height
→ Influence of each parameter

Global SA for Model 1

- Functional global SA[14]: How sensitivity indices (S_i) **evolve over time,** $S_i(t)$

Model 1

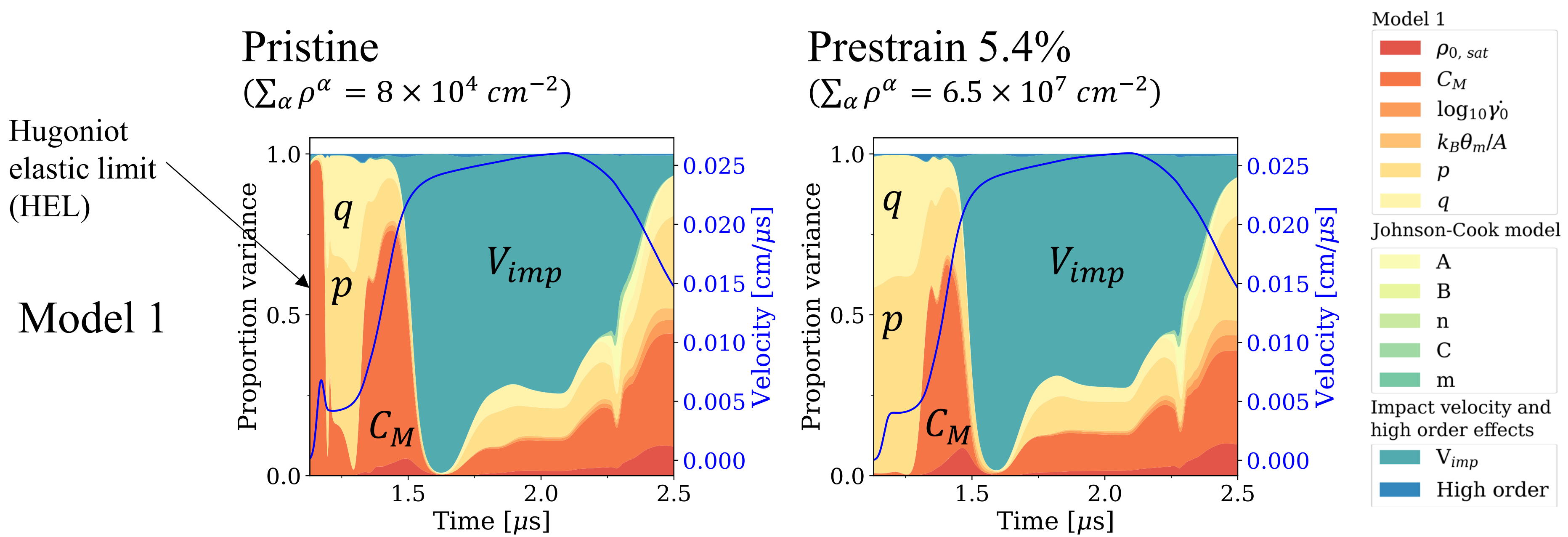

- Pristine: C_M (**Dislocation multiplication**) dominates at the HEL peak
- Prestrained: p and q (**Flow kinetics**) dominate at the HEL peak

Further model refinement: Dislocation nucleation

- Further implications for Model 1

Pristine
($\sum_\alpha \rho^\alpha = 8 \times 10^4\ cm^{-2}$)

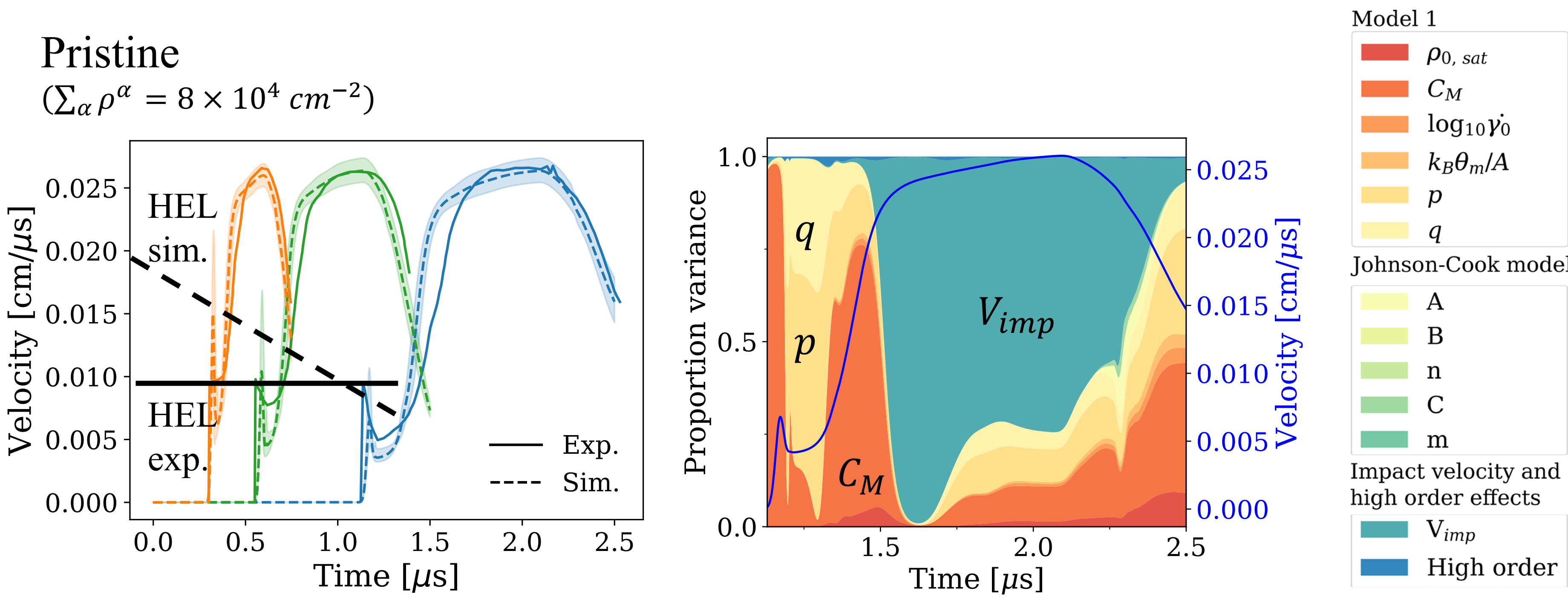

- Diagnosis of the source of the model discrepancy (vs. experiment)

→ At the HEL for the pristine case, C_M is the most influential parameter

→ **Overall variance is determined by C_M → Refine the C_M-related evolution model**

Further model refinement: Dislocation nucleation

- Experiment[12]: **No elastic precursor decay** in pristine [100] Mo
- Simulation: **Shows decay** (overestimates the HEL in thin targets) in pristine [100] Mo

→ Introduced a **thermally activated dislocation nucleation** term[15]

$$\dot{\rho}_M^\alpha = \dot{\rho}_{\text{mult}}^\alpha + \boldsymbol{\dot{\rho}_{nuc}^\alpha} - \dot{\rho}_{\text{ann}}^\alpha - \dot{\rho}_{\text{trap}}^\alpha$$

$$\dot{\rho}_I^\alpha = \dot{\rho}_{\text{trap}}^\alpha - \dot{\rho}_{\text{rec}}^\alpha \approx f_{\text{rec}}^\alpha \dot{\rho}_{\text{trap}}^\alpha$$

$$\dot{\rho}_{\text{nuc}}^\alpha = \dot{\rho}_{n0} \exp\left(-\frac{\Delta G_{n0}}{k_B \theta}\left\langle 1 - \left(\frac{|\tau^\alpha| - \tau_{\text{a}}^\alpha}{\tau_{n0}}\right)^{p_n}\right\rangle^{q_n}\right)$$

- Nucleation term supplies dislocations under the extreme stresses near the impact surface

Further model refinement: Dislocation nucleation

- Experiment[12]: **No elastic precursor decay** in pristine [100] Mo
- Simulation: **Shows decay** (overestimates the HEL in thin targets) in pristine [100] Mo

→ Introduced a **thermally activated dislocation nucleation term**[15]

Pristine

$(\sum_\alpha \rho^\alpha = 8 \times 10^4\ cm^{-2})$

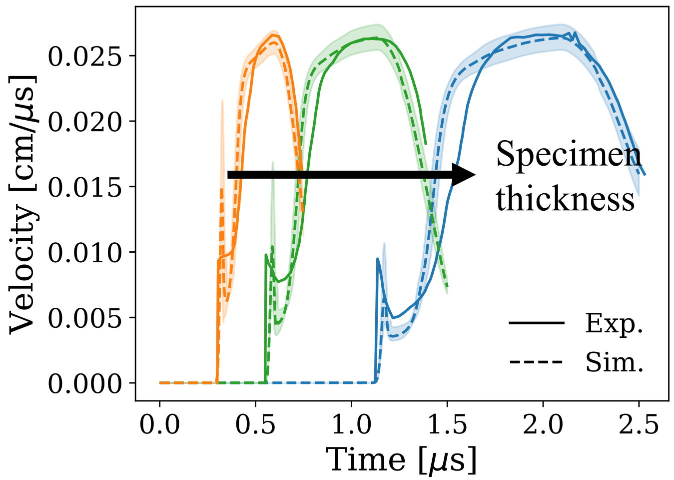

Add $\dot{\rho}^\alpha_{\mathrm{nuc}}$

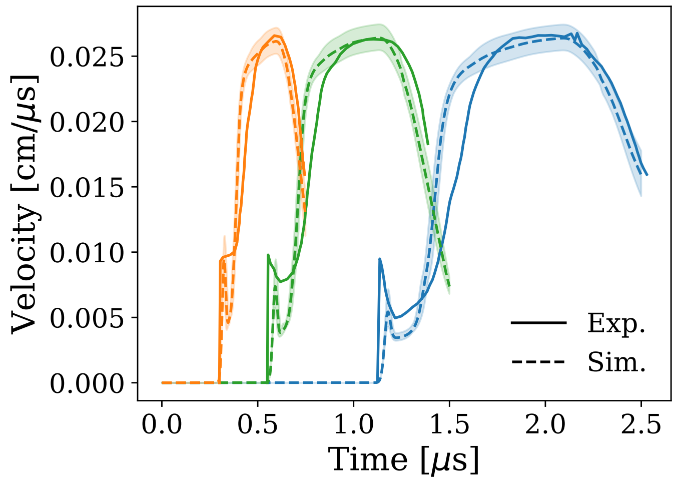

→ Note that the current understanding of nucleation at extreme strain rates remains limited

Conclusion and future work

- **Uncertainty quantification in the modeling of bcc single crystals via Bayesian inference and global sensitivity analysis**

(1) Bayesian calibration

→ Provided probabilistic estimates of parameters in bcc single crystal plasticity models[4, 5]

→ Probabilistic prediction of the deformation behavior both within the calibration regime (stress–strain) and beyond it (plate impact)

(2) Global sensitivity analysis

→ Identified the source of the dislocation-density dependence in the plate impact response

: Mechanism competition between dislocation multiplication and kinetics

→ Guided model refinement based on the sensitivity information

Conclusion and future work

- **Future work**

(1) Identification of deformation and failure mechanisms in bcc single- and polycrystals

→ Ductile damage and spall (void nucleation → growth)

→ Twinning and/or non-Schmid effects at extreme strain rates, and their associated uncertainties

→ Surrogate modeling and uncertainty quantification for large-scale crystal plasticity simulations

(Bronkhorst et al. 2021; Zhang et al. 2023; Schmelzer et al. 2025; Behnoudfar et al. 2026)[16-19]

(2) Extension to amorphous polymeric materials and soft matter

→ Identification of the key physical mechanisms underlying deformation-fracture processes in amorphous polymeric materials in and above the glass transition temperature (T_g)

(Narayan and Anand 2021; J. Lee et al. 2024; Cho et al. 2024)[20-22]

→ Further applications to architected materials on crystal lattices

(Meza et al. 2017; G. Lee et al. 2024; Meyer et al. 2026)[23-25]

Acknowledgement

- This work was supported by the National Research Foundation of Korea (RS-2023-00279843) & Korea Advanced Institute of Science and Technology, South Korea (N11250018, N11240082)

- This work was also performed as a component of LDRD project (LDRD-20230128DR) supported by the US Department of Energy through the Los Alamos National Laboratory

References

[1] Lee, S., Nguyen, T., Luscher, D. J., Fensin, S. J., Carpenter, J. S., & Cho, H. (2026). Bayesian inference and uncertainty quantification for modeling of body-centered-cubic single crystals. *International Journal of Plasticity, 201*, 104678.

[2] Kennedy, M. C., & O'Hagan, A. (2001). Bayesian Calibration of Computer Models. *Journal of the Royal Statistical Society Series B: Statistical Methodology, 63*(3), 425–464.

[3] Higdon, D., Gattiker, J., Williams, B., & Rightley, M. (2008). Computer Model Calibration Using High-Dimensional Output. *Journal of the American Statistical Association, 103*(482), 570–583.

[4] Nguyen, T., Fensin, S. J., & Luscher, D. J. (2021). Dynamic crystal plasticity modeling of single crystal tantalum and validation using Taylor cylinder impact tests. *International Journal of Plasticity, 139*, 102940.

[5] Lee, S., Cho, H., Bronkhorst, C. A., Pokharel, R., Brown, D. W., Clausen, B., Vogel, S. C., Anghel, V., Gray, G. T., & Mayeur, J. R. (2023). Deformation, dislocation evolution and the non-Schmid effect in body-centered-cubic single- and polycrystal tantalum. *International Journal of Plasticity*, 163, 103529.

[6] Madec, R., & Kubin, L. P. (2017). Dislocation strengthening in FCC metals and in BCC metals at high temperatures. *Acta Materialia, 126*, 166–173.

[7] Guiu, F., & Pratt, P. L. (1966). The Effect of Orientation on the Yielding and Flow of Molybdenum Single Crystals. *Physica Status Solidi (b), 15*(2), 539–552.

[8] Guiu, F. (1967). Temperature and Strain Rate Dependence of the Flow Stress in Molybdenum. *Physica Status Solidi (b), 19*(1), 339–351.

[9] Irwin, G. J., Guiu, F., & Pratt, P. L. (1974). The influence of orientation on slip and strain hardening of molybdenum single crystals. *Physica Status Solidi (a), 22*(2), 685–698.

References

[10] Bulatov, V. V., Hsiung, L. L., Tang, M., Arsenlis, A., Bartelt, M. C., Cai, W., Florando, J. N., Hiratani, M., Rhee, M., Hommes, G., Pierce, T. G., & De La Rubia, T. D. (2006). Dislocation multi-junctions and strain hardening. *Nature, 440*(7088), 1174–1178.

[11] Davidson, D. L., Lindholm, U. S., & Yeakley, L. M. (1966). The deformation behavior of high purity polycrystalline iron and single crystal molybdenum as a function of strain rate at 300°k. *Acta Metallurgica, 14*(6), 703–710.

[12] Kanel, G. I., Garkushin, G. V., Savinykh, A. S., Razorenov, S. V., Paramonova, I. V., & Zaretsky, E. B. (2022). Effect of small pre-strain on the resistance of molybdenum [100] single crystal to high strain rate deformation and fracture. *Journal of Applied Physics, 131*(9), 095903.

[13] Sobol', I. M. (2001). Global sensitivity indices for nonlinear mathematical models and their Monte Carlo estimates. *Mathematics and Computers in Simulation, 55*(1–3), 271–280.

[14] Francom, D., & Sansó, B. (2020). BASS: An *R* Package for Fitting and Performing Sensitivity Analysis of Bayesian Adaptive Spline Surfaces. *Journal of Statistical Software, 94*(8).

[15] Armstrong, R. W., Arnold, W., & Zerilli, F. J. (2007). Dislocation Mechanics of Shock-Induced Plasticity. *Metallurgical and Materials Transactions A, 38*(11), 2605–2610.

[16] Bronkhorst, C. A., Cho, H., Marcy, P. W., Vander Wiel, S. A., Gupta, S., Versino, D., Anghel, V., & Gray, G. T. (2021). Local micro-mechanical stress conditions leading to pore nucleation during dynamic loading. *International Journal of Plasticity, 137*, 102903.

[17] Zhang, Y., Chen, N., Bronkhorst, C. A., Cho, H., & Argus, R. (2023). Data-driven statistical reduced-order modeling and quantification of polycrystal mechanics leading to porosity-based ductile damage. *Journal of the Mechanics and Physics of Solids, 179*, 105386.

References

[18] Schmelzer, N. J., Lieberman, E. J., Chen, N., Dunham, S. D., Anghel, V., Gray, G. T., & Bronkhorst, C. A. (2025). Statistical evaluation of microscale stress conditions leading to void nucleation in the weak shock regime. *International Journal of Plasticity, 188*, 104318.

[19] Behnoudfar, P., Ponnana, D. N., Schmelzer, N. J., Wanni, J., Gray, G. T., Thoma, D. J., Bronkhorst, C. A., Chen, N., & Pan, W. (2026). SPLIT-PINN: Separable probability learning technique via physics-informed neural networks for high-dimensional probabilistic modeling. *Journal of the Mechanics and Physics of Solids, 216*, 106777.

[20] Narayan, S., & Anand, L. (2021). Fracture of amorphous polymers: A gradient-damage theory. *Journal of the Mechanics and Physics of Solids, 146*, 104164.

[21] Lee, J., Lee, J., Yun, S., Kim, S., Lee, H., Chester, S. A., & Cho, H. (2024). Size-dependent fracture in elastomers: Experiments and continuum modeling. *Physical Review Materials, 8*(11), 115602.

[22] Cho, H., Lee, J., Moon, J., Pöselt, E., Veld, P. J. I., Rutledge, G. C., & Boyce, M. C. (2024). Large strain micromechanics of thermoplastic elastomers with random microstructures. *Journal of the Mechanics and Physics of Solids, 187*, 105615.

[23] Meza, L. R., Phlipot, G. P., Portela, C. M., Maggi, A., Montemayor, L. C., Comella, A., Kochmann, D. M., & Greer, J. R. (2017). Reexamining the mechanical property space of three-dimensional lattice architectures. *Acta Materialia, 140*, 424–432.

[24] Lee, G., Lee, J., Lee, S., Rudykh, S., & Cho, H. (2024). Extreme resilience and dissipation in heterogeneous elasto-plastomeric crystals. *Soft Matter, 20*(2), 315–329.

[25] Meyer, P. P., Tancogne-Dejean, T., & Mohr, D. (2026). Unified data-driven constitutive modeling of mechanical metamaterials across truss, shell, and plate topologies. *Extreme Mechanics Letters, 83*, 102438.